Journal Pre-proofs

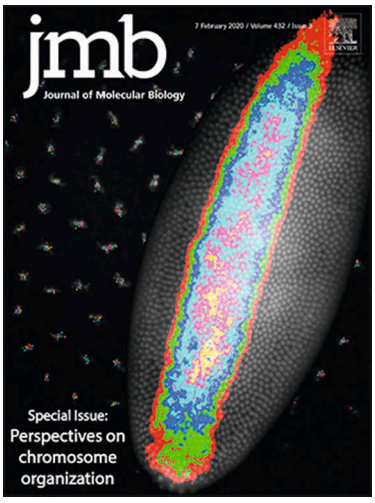

Research Article

NMR structural and biophysical analysis of the disease-linked inner mitochondrial membrane protein MPV17

Laura E. Sperl, Franz Hagn

PII: S0022-2836(21)00322-3
DOI: https://doi.org/10.1016/j.jmb.2021.167098
Reference: YJMBI 167098

To appear in: *Journal of Molecular Biology*

Received Date: 16 April 2021
Revised Date: 19 May 2021
Accepted Date: 3 June 2021

Please cite this article as: L.E. Sperl, F. Hagn, NMR structural and biophysical analysis of the disease-linked inner mitochondrial membrane protein MPV17, *Journal of Molecular Biology* (2021), doi: https://doi.org/10.1016/j.jmb.2021.167098

NMR structural and biophysical analysis of the disease-linked inner mitochondrial membrane protein MPV17

Laura E. Sperl[1] and Franz Hagn[1,2,*]

[1] Structural Membrane Biochemistry, Bavarian NMR Center (BNMRZ) at the Department of Chemistry, Technical University of Munich, Ernst-Otto-Fischer-Str. 2, 85748 Garching, Germany

[2]Institute of Structural Biology, Helmholtz Center Munich, Ingolstädter Landstr. 1, 85764 Neuherberg, Germany

*Correspondence should be addressed to F.H. (phone: +49-89-289-52624, e-mail: franz.hagn@tum.de)

Keywords: dynamics, membrane, mitochondrial diseases, reactive oxygen species, stability, structure

Abstract

MPV17 is an integral inner mitochondrial membrane protein, whose loss-of-function is linked to the hepatocerebral form of the mitochondrial-DNA-depletion syndrome (MDDS), leading to a tissue-specific reduction of mitochondrial DNA and organ failure in infants. Several disease-causing mutations in MPV17 have been identified and earlier studies with reconstituted protein suggest that MPV17 forms a high conductivity channel in the membrane. However, the molecular and structural basis of the MPV17 functionality remain only poorly understood. In order to make MPV17 accessible to high-resolution structural studies, we here present an efficient protocol for its high-level production in *E. coli* and refolding into detergent micelles. Using biophysical and NMR methods, we show that refolded MPV17 in detergent micelles adopts a compact structure consisting of six membrane-embedded α-helices. Furthermore, we demonstrate that MPV17 forms oligomers in a lipid bilayer that are further stabilized by disulfide-bridges. In line with these findings, MPV17 could only be inserted into lipid nanodiscs of 8 to 12 nm in diameter if intrinsic cysteines were either removed by mutagenesis or blocked by chemical modification. Using this nanodisc reconstitution approach, we could show that disease-linked mutations in MPV17 abolish its oligomerization properties in the membrane. These data suggest that, induced by oxidative stress, MPV17 can alter its oligomeric state from a properly folded monomer to a disulfide-stabilized oligomeric pore which might be required for the transport of metabolic DNA precursors into the mitochondrial matrix to compensate for the damage caused by reactive oxygen species.

Introduction

MPV17 is an inner mitochondrial membrane protein (**Fig. 1a**) whose dysfunction has been linked to mitochondrial DNA depletion syndrome, a disease connected to human mitochondrial DNA maintenance defects (MDMD) [1,2]. So far, MDMD has been associated with mutations in 20 different genes, all encoded by the nucleus and involved in either maintenance of the deoxyribonucleotide supply, in the synthesis of mitochondrial DNA (mtDNA) or in mitochondrial fusion [2]. For this rare disease, around 50 different mutations were reported in about 100 patients. In most patients this leads to a hepatocerebral malfunction, such as liver failure [3–5] in early infants. In a few cases mutation in MPV17 resulted in a later-onset neuromyopathic disease with a better prognosis [6–8]. These data show that the clinical outcome correlates with the location of mutations in the MPV17 gene. However, for MPV17 the exact function and underlying pathomechanism is unresolved and the therapy remains merely symptomatic. The protein is known to be crucial for the mtDNA maintenance by conserving a balanced mitochondrial nucleotide pool and has been suggested to act as a transporter for dNTP precursors [4,9]. Consequently, MPV17 deficiency leads to a reduction of dNTPs and DNA in mitochondria, while its overexpression increases the production of reactive oxygen species [4,10,11]. Several MPV17 homologues have been found in the mitochondria of other organisms, including MPV17 in mice and zebrafish, as well as SYM1 in yeast [12–14]. Since these homologues are able to mutually rescue MPV17 function in knockout cells they can serve as valuable model systems to decipher the molecular function of MPV17 [13,15,16]. MPV17 was predicted to consist of four transmembrane helical domains with both termini located in the intermembrane space [11,14]. Furthermore, MPV17 was shown to form a non-selective channel with gating properties [5]. Using electrophysiological methods, MPV17 conductance proved sensitive to changes in the mitochondrial membrane potential, redox state, pH and phosphorylation with a maximal calculated pore size of ~1.8 nm. The channel was found to be closed under conditions

associated with functional mitochondria, which explains how a channel can exist in the inner mitochondrial membrane alongside a high membrane potential [17]. In addition, it has been reported for the yeast homologue SYM1 that the final membrane channel consists of a homo-hexamer or dodecamer [14]. Further studies propose that MPV17 might be a subunit of larger protein complexes (> 600 kDa), suggesting that other membrane proteins are required for pore formation in the inner mitochondrial membrane [12,18].

Despite initial studies on MPV17 function and secondary structure content [17], no higher-resolution structural information is available for this essential membrane protein. In order to obtain a deeper understanding of the mode-of-action of MPV17 and the impact of disease-causing mutations, production and in vitro handling of this membrane protein is required for an in-depth biophysical analysis and structural investigations. Furthermore, bacterial production hosts are particularly attractive and essential for state-of-the-art isotope labeling for high-resolution NMR studies.

Here, we present a protocol for the high-level production of human MPV17 in *E. coli* and show that this membrane protein can be efficiently refolded into detergent micelles. This strategy enables the analysis of the structural features of MPV17 by multidimensional NMR. For this, we performed a screening study for suitable detergents that allow for high-resolution NMR studies and show that MPV17 is properly folded in the best-scoring detergent. Using NMR chemical shift and NOE information, we demonstrate that detergent-solubilized MPV17 is composed of six membrane embedded α-helical secondary structure elements. By utilizing different membrane mimetics, we show that in liposomes MPV17 forms larger oligomeric species that are stabilized by inter-monomer disulfide bridges. However, in lipid nanodiscs of defined sizes [19–21] we show that MPV17 only incorporates into lipid nanodiscs as a monomer if the cysteines in the protein are removed by mutagenesis or blocked by chemical modification. Furthermore, disease-linked MPV17 variants have a decreased tendency to form oligomers. These results show that the oligomeric functional state of MPV17 is stabilized via

inter-subunit disulfide bridges. These features suggest a connection between the redox state in mitochondria and MPV17 channel functionality, which might be required for the transport of nucleotide precursors into the mitochondrial matrix to counteract ROS-induced DNA damage and depletion.

Results

High-level production of MPV17 in *E. coli*

As a first step, we aimed at an optimized production procedure of isotope-labeled MPV17 for subsequent NMR studies. So far, recombinant MPV17 could only be produced in yeast [17]. Despite recent advances in stable isotope labeling in this host [22], the most suitable cell system for this purpose is still *E. coli*, in particular because of the straightforward route to high-level isotope labeling and in particular deuteration, which is a key factor for membrane protein NMR [23]. Thus, we next evaluated the possibility for production of MPV17 in *E. coli*. MPV17 production in *E. coli* without any fusion protein was not successful. Thus, we fused an N-terminal GB1 tag to the protein, which has been shown to enhance production yields and solubility in *E. coli* [24]. For proteolytic removal of the GB1 tag at a later stage in detergent micelles, we inserted a thrombin cleavage site and a GGSS peptide spacer region between GB1 and MPV17 (**Fig. 1b**). This strategy resulted in high production yields of insoluble MPV17 (*inclusion bodies*) and provided a sufficient amount of protein for refolding experiments. For this, we solubilized MPV17 inclusion bodies in the chaotropic agent guanidine hydrochloride (GuHCl) and induced refolding by a dropwise addition into a detergent-containing buffer (**Fig. 1b**). This approach resulted in a homogenous protein preparation as assessed by size exclusion chromatography (**Fig. 1c**) where MPV17 refolded into dodecyl-phosphocholine (DPC) micelles eluted at a volume estimated to have a molecular weight of ~98 kDa. This species contained very pure protein as probed by SDS-

PAGE (**Fig. 1d**). In addition, separation of the cleaved GB1 fusion protein was achieved at that step.

Screening for detergents that are suitable for biophysical and NMR studies

Next, we explored the biophysical and NMR properties of MPV17 in different detergents under reducing conditions, which proved critical for reducing the formation of oligomeric species, as will be discussed below in the section "Probing the oligomeric state of MPV17 in detergent micelles and liposomes". Besides the zwitterionic detergent DPC, that is frequently used for NMR, we evaluated non-ionic detergents, such as C12E8 and maltosides (Cymal-7 and DDM). In all detergents, MPV17 shows a very similar α-helical secondary structure content of ~ 60 %, as probed by far-UV CD spectroscopy (**Fig. 2a**). In addition to the CD spectra, we determined the thermal unfolding traces of MPV17 in these detergents by following the CD signal at 222 nm during heating, which monitors the α-helical secondary structure content, as a readout (**Fig. 2b**). These experiments demonstrated that the apparent stability of MPV17 is lowest in C12E8 (42°C), almost identical in the two maltoside detergents (53 °C) and highest in DPC (73 °C), suggesting that DPC might be a suitable choice for NMR structural investigations at elevated temperatures. The notion that MPV17 is properly folded in DPC micelles is further corroborated by the cooperative thermal unfolding profile of DPC-refolded MPV17 that was subsequently reconstituted into liposomes (**Fig. 2c**), showing a high thermal stability of 63 °C. A protein folding approach to monitor the integrity of MPV17 protein preparations was necessary at this step because no biochemical assay is available so far to assess MPV17 functionality *in vitro*. However, electrophysiological experiments to assess MPV17 pore functionality have been reported previously [14,17]. In one of these studies, MPV17 in DPC micelles was used for membrane incorporation to assemble into a functional channel [17], providing further evidence that MPV17 adopts a proper folding state in DPC. Next, we recorded 2D-[^{15}N,^{1}H]-TROSY NMR spectra to

evaluate the investigated detergents for subsequent multidimensional NMR experiments (**Fig. 2d**). Relevant criteria in this process are the number of resolved NMR signals, which should closely match the number of all non-proline residues in the protein, as well as the homogeneity of the peak intensities. Suitable spectral regions for assessing these criteria are the tryptophane ε NH signals that are well separated from the backbone amide resonances (inset in the spectra in **Fig. 2d**), as well as the glycine backbone amide region at the high-field edge of the ^{15}N dimension (105-110 ppm). In all tested detergents, a decent NMR spectral quality was observed. However, in mild detergents, such as C12E8, Cymal-7 or DDM, MPV17 partially precipitated during the purification process and during the NMR experiment, leading to an additional loss in protein concentration of up to 50%. In contrast, this problem was not encountered in DPC micelles. Furthermore, the number of observed NMR signals in DPC was very close to the expected signals from non-proline residues in the protein (168 of 174). The observed dispersion of NMR signals was very similar in all tested detergents, which supports the assumption that the structure of MPV17 is not markedly influenced by the chosen detergents. Taking into account the excellent spectral quality as well as the large number of well-resolved signals, a more detailed NMR structural characterization of MPV17 was tackled in DPC micelles.

NMR structural characterization of MPV17 in DPC micelles

For the backbone resonance assignment, we recorded a set of 3D TROSY-based triple resonance experiments, consisting of HNCO, HN(CA)CO, HNCA, HN(CO)CA, HNCACB, HN(CO)CACB and a ^{15}N-edited-[^{1}H,^{1}H]-NOESY experiment with a *U*-[^{2}H, ^{13}C, ^{15}N]-labeled MPV17 sample in DPC micelles. The quality of these 3D NMR spectra was sufficient to assign 89% of the backbone amide resonances in the protein (**Fig. 3a)**, as demonstrated by representative strips of a tr-HNCA experiment (**Fig. 3b**). This enabled an almost complete estimation of the secondary structure content based on ^{13}C secondary chemical shift

information (**Fig. 3c**). The Cα and Cβ shifts indicate an α-helix content of ~ 65%, confirming the CD structural data. As compared to a secondary structure prediction based on the amino acid sequence in the protein databank (UniProtKB, entry P39210), the location of α-helices as determined here experimentally shows marked differences. In particular, the short α-helix at the N-terminus (aa 2-14) as well as the longer C-terminal α-helix (aa 153-173) are not present in the prediction, giving rise to only four instead of six α-helices. The herein detected content and location of helical secondary structure elements is most likely also present in other mammalian MPV17 homologues as estimated from the very high sequence identity (**Fig. 3e**). Variations mainly occur outside of the herein determined secondary structure elements. However, structural information is not available for other MPV17 homologues so far. In order to obtain information on the dynamics of MPV17 in the ns to ps time scale, we recorded a $\{^{1}H\}$-^{15}N heteronuclear NOE experiment (**Fig. 3d**). The ^{15}N-hetNOE adopts low values for residues in flexible regions of the protein and values close to 1 for rigid residues. The obtained pattern is in good agreement with the location of α-helical secondary structure elements assuming that flexible residues are mainly located in loop regions. In line with that notion, the calculated order parameter profile based on chemical shift information agrees well with the ^{15}N-hetNOE results. Of particular interest for a putative redox regulated protein such as MPV17 is the presence and the location of cysteine residues. As indicated in **Fig. 3c**, all four cysteine residues (C59, C99, C103, C160) are located in α-helical secondary structure elements and do not show enhanced dynamics in the ns to ps time scale (high ^{15}N-hetNOE values). The α-helical geometry also suggests that C99 and C103 are pointing toward the same side in α-helix 4, which could be relevant for the formation of inter- or intra-monomer disulfide bridges within the membrane.

Location of MPV17 in DPC micelles

Next, we utilized NMR paramagnetic relaxation enhancement experiments to obtain information on the location of the secondary structure elements of MPV17 in the DPC micelle. We compared the NMR peak intensities of backbone amides of MPV17 in DPC micelles with the ones obtained after the addition of a paramagnetic agent (**Fig. 4a,b**). Gd^{3+}-chelated DOTA is soluble in aqueous solution, thus its paramagnetic properties should affect only residues that are located outside the membrane. In contrast, the spin-labeled fatty acid 16-doxyl-stearic acid (16-DSA) incorporates into DPC micelles and consequently affects residues of MPV17 that are located in the membrane region. Looking at the intensity plot obtained with Gd^{3+}-chelated DOTA (**Fig. 4c**), mainly signals that correspond to residues in regions in MPV17 that are not located in secondary structure elements are affected. Only helix 5 seems to be more heavily affected than the other helices. The presence of 16-DSA (**Fig. 4d**) leads to pronounced intensity changes in helical secondary structure elements. In line with the data obtained with DOTA, helix 5 is less affected by 16-DSA. Of particular interest is the notion that all cysteine residues are heavily affected by 16-DSA and thus it can be assumed that they are located inside the hydrophobic membrane area.

Insertion of MPV17 into lipid nanodiscs

Since oligomeric pore assemblies have been proposed for MPV17 and its homologues [14,17] we next set out to investigate the oligomerization properties of MPV17 by assaying the insertion of MPV17 into lipid nanodiscs of defined sizes [19–21,25]. In case large and stable oligomeric species are formed in a lipid bilayer environment, insertion into the selected lipid nanodiscs of 8 -12.5 nm diameter would not be possible. Sterically, insertion is only possible in case of a monomer or smaller oligomeric species. For this scenario we used our previously established GB1 proteolysis assay to quantify the average number of MPV17 monomers in each nanodisc [26]. As outlined in **Fig. 5a**, MPV17 fused to a GB1 protein tag in detergent micelles is used as a starting material. Once the fusion protein is inserted into nanodiscs, these

MPV17-containing nanodiscs are separated from the empty ones by affinity purification and size exclusion chromatography (SEC). Afterwards, thrombin is added to cleave off the GB1-tag. The ratio of GB1 and nanodiscs is calculated by using the absorption peak integrals in a second SEC run. With these data, the number of MPV17 in nanodiscs can be quantified. Using MPV17wt, nanodisc assembly, even with larger nanodiscs (12.5 nm) was not successful, suggesting the formation of a large oligomeric species in a lipid environment. Thus, we removed all four cysteine residues in the protein, yielding MPV17ΔCys. In agreement with the assumption that cysteine residues play a crucial role in MPV17 oligomerization, the MPV17ΔCys could successfully be incorporated into lipid nanodiscs of various sizes (**Fig. 5b,d**). The average number of MPV17ΔCys per MSP1ΔH5 nanodisc (8 nm diameter [19]) was determined to be 1.45, which suggests that even without cysteine residues MPV17 has a tendency to oligomerize, even at lipid nanodisc assembly conditions that would favor the incorporation of a monomer (**Fig. 5d**). An almost identical behavior (1.42 MPV17 per MSP1ΔH5 nanodisc) could be detected if the cysteines in MPV17wt had been chemically blocked by the methylation reagent MMTS (**Fig. 5b,d**). The usage of larger nanodiscs and of MPV17-to-MSP ratios theoretically leading to the incorporation of more than one MPV17 resulted in the incorporation of on average almost three MPV17 monomers. In these experiments a slight effect of the lipid composition on MPV17 oligomerization could be observed. The negatively charged and dimeric lipid cardiolipin (CL) that is highly abundant in the inner mitochondrial membrane appears to hinder the incorporation of an oligomer. In particular, this is apparent with small MSP1ΔH5 nanodiscs, where the usage of CL results in only half as much MPV17 in nanodiscs as the negatively charged monomeric lipid DMPG. This behavior can be rationalized by tight binding of CL to MPV17, leading to a larger preformed protein-lipid assembly that is too large for the 8 nm nanodiscs if higher oligomers are present. In order to assay the MPV17 folding state, we performed CD-detected thermal unfolding experiments with the nanodiscs shown in **Fig. 5c**. Both MPV17 species show a

thermal stability of around 60 °C followed by the unfolding transition of the MSP at > 70 °C. This is in excellent agreement with the thermal stability of MPV17wt in liposomes (T_m = 62 °C, **Fig. 2c**). In addition to the CD-spectroscopic analysis, we inserted ^{2}H,^{15}N-labeled MPV17ΔCys into MSP1ΔH5 nanodiscs and recorded a 2D-[^{15}N,^{1}H]-TROSY spectrum (**Fig. 5e**). The obtained spectrum (blue contour lines) showed a very similar backbone amide signal dispersion as in DPC micelles (grey contour lines), indicating that the overall structure of the MPV17 monomer is not heavily altered by the chosen membrane mimetic. In addition, we could not obtain a purely monomeric MPV17 nanodisc preparation, which introduces an additional portion of heterogeneity and consequently line broadening in NMR experiments. Furthermore, taking into account the proposed oligomeric functional form of MPV17, it seems likely that monomeric MPV17 trapped in small lipid nanodiscs would show an enhanced level of exchange dynamics in the intermediate regime as compared to a more stable oligomer, further leading to line broadening effects. Thus, we assume that the monomeric form of MPV17 represents the inactive species that, upon stimulation, needs to assemble into more stable membrane pores.

Structural effects of cysteine removal or modification

In order to obtain a better understanding of the role of the cysteine residues for the MPV17 structure, we performed a sequence specific NMR backbone resonance assignment of methylated MPV17wt (met-MPV17wt) as well as MPV17ΔCys in DPC micelles (**Fig. 6a,b**). The backbone amide signal positions in a 2D-[^{15}N,^{1}H]-TROSY experiment were then compared with MPV17wt using chemical shift perturbation (CSP) plots. For met-MPV17wt (**Fig. 6c**), the CSP effects are relatively broadly distributed around the modified cysteine residues. Apparently, the incorporation of an additional -SCH_3 moiety leads to minor steric clashes as well as to changes in the electronic properties of the cysteine residues, which more heavily affects neighboring regions. In contrast, the CSP pattern for MPV17ΔCys (**Fig. 6d**) is

very sharply clustered around the mutated cysteine residues. All cysteines were mutated to alanine, leading only to subtle changes in the electronic properties in close proximity to the mutation sites. This indicates that the overall fold is not changed by the elimination of cysteines. To confirm these findings, we assayed the thermal stability of MPV17wt and MPV17ΔCys in DPC micelles using CD spectroscopy. In these experiments, we could detect an only slightly increased stability for MPV17wt (**Fig. 6e**) as compared to MPV17ΔCys (**Fig. 6f**), confirming that the cysteine residues do not play a critical role for the folding and the stability of the MPV17 monomer.

Probing the oligomeric state of MPV17 in detergent micelles and liposomes

Since the presented data suggest that the cysteine residues of MPV17 play a role in its oligomerization, even in DPC micelles, we next wanted to probe the oligomerization behavior in this membrane mimetic and in more native liposomes using crosslinking assays. First, we utilized the oxidizing agent Cu^{2+}-phenanthroline $(Phen)_2$-Cu^{2+} to monitor the cysteine-dependent crosslinking of MPV17wt (**Fig. 7a**) in DPC micelles and POPC:CL liposomes. In the absence of reducing agents, MPV17 showed a clear band for a dimer in DPC micelles and the addition of $(Phen)_2$-Cu^{2+} did not reveal further oligomeric species. In contrast, in liposomes almost no oligomeric species was visible without the oxidizing agent, must likely due to a shorter storage time before the crosslinking was performed. However, once $(Phen)_2$-Cu^{2+} was added, the formation of a dimer but also of higher oligomeric species could be detected in liposomes. This data clearly shows that the cysteines are accessible for disulfide-bond formation, leading to oligomerization induced by oxidative stress. To verify these results, we performed crosslinking with the amino-selective crosslinker BS^3. This enabled us to investigate the occurrence of oligomers in the absence or presence of a reducing agent (**Fig. 7b**). In the presence of the reducing agent dithiothreitol (DTT), predominantly the monomeric form could be detected for MPV17 in DPC micelles. Also in liposomes, the addition of DTT

resulted in a marked reduction of oligomers with only the dimer giving rise to a clearly visible band on the SDS-PAGE gel. In the absence of DTT, BS^3 revealed large oligomeric species in liposomes as seen for the cysteine-mediated crosslinking experiments. These data further highlight the role of MPV17 as a redox-regulated protein - a conclusion additionally supported by NMR experiments at reducing and non-reducing conditions using $^{2}H,^{15}N$-labeled MPV17 in DPC micelles. As already shown in **Fig. 3a**, MPV17 gives rise to a well resolved spectrum under reducing conditions (**Fig. 7c, left**), whereas marked line broadening and signal disappearance can be observed in the absence of a reducing agent (**Fig. 7c, left**). A more detailed analysis of the peak intensities under both conditions shows that mostly residues are affected that are located in those regions where cysteines are present (**Fig. 7d**). The pronounced effects detected in the NMR experiments suggest the formation of dimers or even larger oligomers, favored by the more than 10-fold higher concentration as compared to the cysteine-dependent crosslinking experiments (**Fig. 7a**).

Several mutations in MPV17 are linked to diseases such as the hepatocerebral form of the mitochondrial-DNA-depletion syndrome (MDDS) [1,2]. Thus, assuming that MPV17 functionality is heavily linked to its oligomeric state, we set out to investigate the oligomerization tendencies of three of the disease-related mutations (R50W, Q93P and N166K [11,27]) in our lipid nanodisc assay (**Fig. 7e**). In this set of experiments, we could incorporate a small amount of MPV17wt into MSP1ΔH5 lipid nanodiscs if very high amounts of DTT were added (> 20 mM) (black SEC trace). However, even under these strongly reducing conditions, the assembly yield was too low for a more detailed analysis. However, nanodisc assembly yields with the disease variants of MPV17 were much higher, especially with the R50W and Q93P variants, suggesting that these mutations indeed lead to a marked weakening of the oligomerization tendency of MPV17. A quantification of the number of MPV17 protomers in each MSP1ΔH5 nanodisc (**Fig. 7e**) showed that only one MPV17 was present with all tested variants. This number is lower than the number obtained with

MPV17ΔCys or met-MPV17wt (see **Fig. 5**), most likely because the investigated mutations disturb the interaction between the individual MPV17 monomers, leading to the expected insertion of one monomer under assembly conditions that strongly favor this stoichiometry. This data also suggests that inter-monomer disulfide-bond formation only takes place if MPV17 is able to initially interact in a non-covalent manner. In line with this notion is that mutations of single cysteine residues are not among the known disease linked MPV17 variants.

Discussion

In this study we demonstrate that the inner mitochondrial membrane protein MPV17 can be produced efficiently in *E. coli* and refolded into detergent micelles (**Fig. 1**). The herein described protocol will facilitate the high-level production of MPV17 for further biochemical, biophysical and structural investigations. In particular, it enables further NMR studies since *E. coli* permits cutting-edge isotope labeling schemes that are required for the structure determination of large membrane proteins [23].

Additionally, we here present a systematic biophysical approach for the identification of optimized detergent conditions that enable high-resolution NMR studies. Using a combination of size exclusion chromatography, CD and NMR spectroscopy with refolded MPV17, we could identify DPC as the detergent in which MPV17 behaved most favorable (**Fig. 2**). In DPC, MPV17 shows a high thermal stability and does not tend to precipitate during NMR experiments at 37 °C. This was essential for obtaining an almost complete NMR backbone resonance assignment. This initial NMR work will serve as a promising starting point for a more detailed NMR or EM structural analysis of MPV17 in detergent micelles or other membrane mimetics, such as lipid nanodiscs of varying sizes in order to incorporate monomeric or oligomeric pore forming species [19–21,25].

The NMR characterization presented here permits the mapping of α-helical secondary structure elements leading to the identification of six α-helical elements (**Fig. 3**).

Furthermore, it has been shown that MPV17 or the yeast homologue Sym1 form oligomeric pore structures in a lipid bilayer membrane [14,17] and this assembly is most likely induced by oxidative stress in the mitochondrial matrix [17]. These functional features suggest that cysteine residues might play a crucial role for MPV17 oligomerization and eventually membrane pore formation. Human MPV17 contains four cysteine residues at positions 59, 99, 103 and 160. With our NMR data, we could show that all cysteines are positioned in α-helical secondary structure elements in the protein (**Fig. 3b**) and these regions are located inside the hydrophobic interior of the detergent micelle (**Fig. 4**), suggesting that stable oligomerization of MPV17 is mediated by disulfide bond formation within the membrane. Recently, it has been shown that MPV17 produced in the yeast strain *Pichia pastoris* and extracted and purified in DPC micelles could be functionally reconstituted into lipid bilayers for electrophysiological experiments [17]. These data clearly support our conclusion that MPV17 preparations in DPC micelles are properly folded and capable of forming a redox-sensitive channel in a lipid bilayer membrane. In that study five out of the six α-helices were predicted and a very similar size exclusion chromatography profile and far-UV CD spectrum could be obtained.

Using our established nanodisc insertion assay [26], we showed that cysteine residues are key elements for stable oligomerization in the membrane. Wild-type MPV17 could not be inserted into nanodiscs ranging from 8 to 12.5 nm in size, whereas cysteine-deficient or cysteine-methylated MPV17 behaved much better in this assay (**Fig. 5**). However, even without available cysteine sulfhydryl moieties, MPV17 had a slight tendency to form oligomeric species, manifested in on average more than one inserted MPV17 monomer under nanodisc assembly conditions that strongly favor the insertion of a monomer, i.e., with a large excess of empty nanodiscs in the assembly mixture. In this almost monomeric nanodisc-incorporated

state, MPV17 shows a high degree of conformational flexibility, as evident from the strong line-broadening effects in 2D-NMR experiments of MPV17ΔCys in MSP1ΔH5 nanodiscs (**Fig. 5e**). The mutation of cysteine residues does not lead to strong NMR spectral changes, indicating that folding of the MPV17 monomer is not dependent on the formation of intra-molecular disulfide bridges. In line with this notion, we found that the thermal stability of MPV17 is only slightly lower if cysteine residues are removed (**Fig. 6**).

For our NMR studies, the use of detergent micelles was critical because MPV17 strongly tends to oligomerize in a lipid bilayer environment (**Fig. 7**) and this oligomeric form might indeed be the functionally active species that forms at oxidative stress conditions. For the yeast homologue Sym1, oligomeric assemblies corresponding to a 6- and 12-mer have been detected by blue-native PAGE [14]. In line with these previous observations, we here detected oligomers up to a hexamer in our crosslinking assay. The ability of MPV17 to form disulfide-linked larger species can also be observed by NMR spectroscopy in DPC micelles if reducing agents are omitted and the protein is present in a relatively high concentration (**Fig. 7c**).

Finally, we investigated the impact of disease-linked mutations on the formation of oligomeric states. The expectation for a disease-causing mutation would be that MPV17 oligomerization and eventually pore formation is markedly reduced. An earlier study revealed that disease-linked mutations in the yeast homologue Sym1 reduce the amount of higher molecular weight complexes, suggesting that the mutations hamper its oligomerization [28]. As shown in **Fig. 7e**, the anticipated behavior was observed with the investigated MPV17 variants R50W, Q93P, N166K. To a varying extent, all of these variants can be inserted into small lipid nanodiscs, which was almost impossible with the wild-type protein. Of note, these variants insert into nanodiscs as a pure monomer, which is in contrast to MPV17 where cysteines have been either removed or blocked. This behavior suggests that MPV17 needs to oligomerize in a non-covalent manner before cysteine residues of neighboring monomers are able to form disulfide bridges.

With the herein presented data we can further refine our understanding of the molecular features of MPV17 and its functional role in the inner mitochondrial membrane. Earlier studies showed that MPV17 is forming a membrane pore upon the exposure to oxidative stress [17]. We here show that oligomerization, which is most likely linked to pore formation, is stabilized via disulfide bonds. Among other possible effects, disease causing mutations can lead to a weakening of MPV17 oligomerization, which would most likely prevent stable pore formation. These insights suggest that the MPV17 pore is important under oxidative stress conditions that can easily occur in the mitochondrial matrix as the site of oxidative phosphorylation, where reactive oxygen species (ROS) are generated. It has been proposed that diseases like mitochondrial DNA depletion syndrome (MDDS) are linked to ROS stress [11]. A possible explanation for this observation might be that ROS lead to increased mitochondrial DNA damage, increasing the demand for nucleotide precursors to be imported into the mitochondrial matrix (**Fig. 8**). Since MPV17 is located in the inner mitochondrial membrane, it can directly sense buildup of reactive oxygen species and form a channel that can (selectively) transport the required metabolic precursors. If the MPV17 channel cannot be formed due to a critical mutation in the protein, damaged DNA cannot be repaired or synthesized, leading to its gradual depletion.

In conclusion, we here provided novel structural and function insights on the disease-linked mitochondrial membrane protein MPV17. Furthermore, we presented production protocols in bacterial hosts that will be helpful for a more detailed structural characterization of the MPV17 monomer as well as the final oligomeric pore state at high resolution. Such studies will be essential for obtaining a better mechanistic understanding of the regulation and selectivity of MPV17 under varying cellular stress conditions.

Experimental Procedures

Construct design and production of MPV17 in E. coli

The MPV17 gene was cloned into a pET15b vector harboring a N-terminal His_6-tag, followed by a GB1 fusion protein and a thrombin protease cleavage site. Cysteine-free (C59A, C99A, C103A, C160A) or disease-linked single point variants (R50W, Q93P, N166K) of MPV17 were obtained by site directed mutagenesis using a Quikchange lightning mutagenesis kit (Stratagene). *E. coli* BL21 (DE3) cells were transformed with the respective plasmid and grown in shaker flasks at 37°C. After reaching an OD_{600} of 0.6-0.8, protein expression was induced with 0.1 mM IPTG and the cells were shaken for an additional 4h. For the production of [*U*-^{2}H, ^{13}C, ^{15}N]-MPV17, bacteria were grown in M9 medium supplemented with 1 g/L [98% ^{15}N]-NH_4Cl and 2 g/L [98% ^{2}H, ^{13}C]-glucose in 99% D_2O (Eurisotope or Sigma-Aldrich). MPV17 accumulated in the insoluble fraction as inclusion bodies.

Purification of MPV17

The MPV17 protein pellet, produced in *E. coli*, was resuspended in lysis buffer (50 mM Tris pH 8.0, 200 mM NaCl, 1 mM EDTA, 1 mM PMSF) and incubated with lysozyme for 30 min. Cells were lysed by sonicating for 10 min (1 s on, 2 s off, 30% amplitude; Sonifier 250D, Branson). The lysate was incubated with DN*ase* I and 5 mM $MgCl_2$ for 30 min and cleared by centrifugation (50.000 g, 30 min, 4 °C). The pellet was washed once with wash buffer A (20 mM Tris pH 8.0, 100 mM NaCl, 1 mM EDTA) + 1 % TritonX-100 and twice with buffer A. The resulting pellet containing inclusion bodies was dissolved in buffer B (50 mM Tris pH 8, 6 M GdmCl, 5 mM beta-mercaptoethanol (BME)) + 1 mM $MgCl_2$. The protein solution was purified on a Ni-NTA gravity flow column equilibrated in buffer B, washed with 10 CV buffer B + 10 mM imidazole and eluted with 5 CV buffer B + 500 mM imidazole. The elution fraction was dialyzed against 5 L of 10 mM Tris pH 8.0, 1 mM EDTA, 5 mM BME, resulting in precipitation of MPV17. The precipitate was dissolved in 50 mM Tris pH 8.0, 6 M GdmCl,

100 mM NaCl, 5 mM EDTA, 10 mM DTT at a protein concentration of 5 mg/mL. Refolding of MPV17 into detergent micelles was done by dropwise addition of the protein solution into a 10-fold excess of refolding buffer (0.5 % DPC (or other detergent), 20 mM NaPi pH 7.0, 200 mM NaCl, 1 mM EDTA, 5 mM DTT) and dialyzed against 2 L of 20 mM Tris pH 8.0, 100 mM NaCl, 2 mM DTT to remove residual GdmCl. For GB1 removal, 100U Thrombin was added and incubated at room temperature for 3-4 h. Finally, MPV17 was purified on a HiLoad 16/600 Superdex 200 pg size exclusion column (GE Healthcare) in 20 mM NaPi pH 7.0, 50 mM NaCl, 1 mM EDTA, 0.1 % DPC (or other detergent), 5 mM DTT.

Cysteine-specific methyl labeling with S-methyl-methanethiosulfonate (MMTS)

MMTS labeling was done according to a published protocols [29] with specific modifications required for a membrane protein [30]. After chromatographic separation by a semi-preparative S200 (300/10) column the pooled fractions were concentrated in Amicon 15 centrifugal devices (10,000 MWCO) to approx. 250 µL and washed with 3 x 12.5 mL methyl labelling buffer (50 mM NaPi pH 7.5, 1 mM EDTA, 0.1% DPC (w/v) to remove the reducing agent DTT. After buffer exchange, 1 mL of protein sample was transferred to a reaction tube and the exact concentration of the protein sample was determined by UV/Vis spectroscopy for subsequent S-methyl-methanethiosulfonate (MMTS) labeling. The concentration of MMTS (Sigma-Aldrich, 100 mM stock in DMSO) was adjusted to a 5-fold molar excess per cysteine residue in MPV17 and the mixture was incubated overnight at 4 °C on a rotating mixer. Subsequently methyl labeled MPV17 was washed with 3 x 12.5 mL NMR buffer (20 mM NaPi pH 7.0, 50 mM NaCl, 0.5 mM EDTA, 0.1 % DPC (w/v)) to remove the remaining free MMTS reagent.

Nanodisc assembly

Nanodiscs were assembled with the MPV17 to MSP ratios indicated for the individual assemblies according to established protocols [19–21]. ΔH5-nanodiscs were formed by applying an MSP to lipid ratio of 1:25 [31], while 1E3D1-nanodiscs were formed using an MSP to lipid ratio of 1:85 (80 for the 1:1 ratio of MPV17:MSP) [25]. As lipids either DMPC/DMPG (75/25) or DMPC/Cardiolipin (14:1) (80/20) were used. The mixtures were assembled in 20 mM Tris pH 7.5, 100 mM NaCl, 0.5 mM EDTA (for MPV17wt and cysteine containing variants, 10 mM DTT was added) for 1.5 h at room temperature with a final MSP concentration of 150 µM. 0.6g/mL of Biobeads-SM2 (Biorad) were added and the assembly was shaken at room temperature for 3.5 h. Finally, the MPV17 containing nanodiscs were separated by Ni-NTA affinity chromatography and subjected to SEC. Thrombin cleavage was performed at 37 °C for 4 h, followed by a second SEC performed to separate the cleaved GB1. The ratio of MPV17/nanodisc was calculated from the resulting chromatogram as described before [26].

Liposome preparation

3 mg of POPC (palmitoyl-oleoyl-glycero-phosphocholine) and 1.5 mg of Cardiolipin (18:1) (both obtained from Avanti Polar Lipids) were mixed in chloroform and dried under a N_2 gas stream. The lipids were resuspended in 500 µL of liposome buffer (20 mM NaPi pH 7.0, 50 mM NaCl, 0.5 mM DTT), subjected to 8 freeze/thaw cycles and extruded 11 times through a filter with 100 nm pore size. MPV17 in DPC was added at a protein to lipid ratio of 1:500. After incubation for 30 min at 4 °C, the liposomes were dialyzed overnight at 4 °C in a 10 kDa MWCO membrane against 1 L of liposome buffer.

Crosslinking

For cysteine-mediated crosslinking with the oxidizing agent Cu/Phe, both MPV17-containing liposomes and MPV17 in DPC-micelles were dialyzed in a 10 kDa MWCO membrane against

20 mM Tris pH 8.0, 50 mM NaCl for 3 h at RT. The Cu/Phe reagent was prepared freshly before usage as described previously [32]. This resulted in a 240 mM stock solution in EtOH:H_2O (1:4), followed by two steps of 1:10 dilution in H_2O. 30 µM of Cu/Phe was added to MPV17 containing samples (10 or 20 µM) and incubated for 1 h at 25 °C while shaking. The resulting protein species were monitored with a non-reducing SDS-PAGE.

For BS^3-crosslinking a 25 mM BS^3 (suberic acid bis(3-sulfo-N-hydroxy-succinimide ester) sodium salt) solution was prepared freshly in BS^3 buffer (20 mM NaPi pH 7.0, 50 mM NaCl). The liposome samples were prepared by either dialyzing against BS^3 buffer or adding 20 mM DTT to the liposome buffer. MPV17 in DPC micelles was used directly after SEC. Samples were diluted to 20 µM in the respective buffer and the BS^3-crosslinker was added at a 1:30 ratio. The reaction was performed at 25°C for 1h under shaking. The result analyzed with SDS-PAGE and Coomassie staining.

Circular dichroism (CD) spectroscopy

CD measurements were conducted on a Jasco J-715 spectropolarimeter with a 1 mm path-length quartz cuvette. Spectra were measured at 20 °C. Thermal unfolding was measured by monitoring the ellipticity at 222 nm between 20 and 100 °C with a heating rate of 1 °C/min. Data were fitted to a custom Boltzmann equation for thermal unfolding [33].

NMR spectroscopy

NMR experiments were done at 310 K on Bruker AvanceIII spectrometers operating at 600, 800, 900 and 950 MHz proton frequency, respectively, with cryogenic probes and controlled by Topspin 3.5 (Bruker Biospin). For backbone resonance assignments, a set of TROSY-type 3D-experiments was recorded [34] as well as a 3D-^{15}N-edited-[^{1}H,^{1}H]-NOESY-TROSY (200 ms mixing time) with ~ 400 µM *U*-^{2}H,^{13}C,^{15}N-labeled MPV17 samples (wt, cysteine-free, MMTS methylated) in 20 mM NaPi, pH 7.0, 50 mM NaCl, 0.5 mM EDTA, 5 mM DTT (only

wt MPV17), 300 mM DPC (Anatrace, F308) were run in a non-uniformly sampled (NUS) manner with 15-20 % sampling density. The NUS sampling schedule was obtained by the Poisson-gap method [35]. For rapid spectra reconstruction, we employed iterative soft thresholding (IST) [36]. All NUS-3D spectra were processed with NMRpipe [37]. All other spectra were processed with Topspin3.5 (Bruker Biospin). Resonance assignment and NMR data analysis was done with NMRFAM-Sparky [38]. Chemical shift-based order parameters were calculated with the program TALOS+ [39]. Chemical shift perturbations were calculated as ^{1}H,^{15}N-averaged values, as described in Ref. [40] using the perturbation analysis module in NMRFAM-Sparky [38].

{^{1}H},^{15}N-heteronuclear NOE was measured with a 400 µM ^{2}H,^{15}N-labeled sample at 310K with a 2 s proton saturation time, 96 transients and 128 complex points in the indirect ^{15}N dimension in a fully interleaved manner.

Paramagnetic relaxation enhancement (PRE) experiments were conducted with a series of 2D-[^{15}N,^{1}H]-TROSY experiments (recycle delay 2 s) with or without the paramagnetic agent. For probing membrane locations, we added spin-labeled 16-doxyl-stearic acid (16-DSA) to a ^{2}H,^{15}N-labeled MPV17 sample in DPC micelles at 1 to 5 mM concentration. For measuring solvent PREs, soluble Gd^{3+}-DOTA was stepwise added to the MPV17 sample in DPC micelles at a final concentration of 2 to 8 mM. At each sample, a 2D-[^{15}N,^{1}H]-TROSY experiment was recording with a recycle delay of 2 s.

Data availability

The NMR backbone resonance assignments of MPV17wt, cysteine-free MPV17 and MMTS-labeled MPV17wt in DPC micelles have been deposited at the BMRB databank (acc. codes 50889, 50890, 50891). All other data are contained in the manuscript.

Acknowledgments

The authors want to thank Maximilian Schneider (TUM) for the initial optimization of nanodisc assemblies containing MPV17, and Drs. Gerd Gemmecker and Sam Asami (BNMRZ) for general NMR support. We acknowledge spectrometer time at the Bavarian NMR Center (BNMRZ, www.bnmrz.org).

Author contributions

L.E.S. produced proteins, conducted biophysical and NMR experiments and analyzed data. F.H. performed NMR experiments and data analysis and supervised the study. Both authors wrote the manuscript.

Funding and additional information

This study was supported by the Helmholtz Society (to F.H., no. VG-NG-1035) and the Technical University of Munich, Institute for Advanced Study, funded by the German Excellence Initiative and the European Union Seventh Framework Programme under grant agreement n° 291763, as well as the Center for Integrated Protein Science Munich (CIPS^{M}). Requests for materials should be addressed to F.H.

Conflict of interest

The authors declare that they have no conflicts of interest with the contents of this article.

References

[1] W. Copeland, Defects in Mitochondrial DNA Replication and Human Disease, Crit Rev Biochem Mol Biol. 47 (2012) 64–74. https://doi.org/10.1161/CIRCULATIONAHA.110.956839.

[2] A.W. El-Hattab, W.J. Craigen, F. Scaglia, Mitochondrial DNA maintenance defects, Biochim. Biophys. Acta - Mol. Basis Dis. 1863 (2017) 1539–1555.

https://doi.org/10.1016/j.bbadis.2017.02.017.

[3] L.-J.C. Wong, N. Brunetti-Pierri, Q. Zhang, N. Yazigi, K.E. Bove, B.B. Dahms, M.A. Puchowicz, I. Gonzalez-Gomez, E.S. Schmitt, C.K. Truong, C.L. Hoppel, P.-C. Chou, J. Wang, E.E. Baldwin, D. Adams, N. Leslie, R.G. Boles, D.S. Kerr, W.J. Craigen, Mutations in theMPV17 gene are responsible for rapidly progressive liver failure in infancy, Hepatology. 46 (2007) 1218–1227. https://doi.org/10.1002/hep.21799.

[4] A.W. El-Hattab, J. Wang, H. Dai, M. Almannai, C. Staufner, M. Alfadhel, M.J. Gambello, P. Prasun, S. Raza, H.J. Lyons, M. Afqi, M.A.M. Saleh, E.A. Faqeih, H.I. Alzaidan, A. Alshenqiti, L.A. Flore, J. Hertecant, S. Sacharow, D.S. Barbouth, K. Murayama, A.A. Shah, H.C. Lin, L.J.C. Wong, MPV17-related mitochondrial DNA maintenance defect: New cases and review of clinical, biochemical, and molecular aspects, Hum. Mutat. 39 (2018) 461–470. https://doi.org/10.1002/humu.23387.

[5] A. Spinazzola, R. Santer, O.H. Akman, K. Tsiakas, H. Schaefer, X. Ding, C.L. Karadimas, S. Shanske, J. Ganesh, S. Di Mauro, M. Zeviani, Hepatocerebral Form of Mitochondrial DNA Depletion Syndrome, Arch. Neurol. 65 (2008) 1108–1113. https://doi.org/10.1001/archneur.65.8.1108.

[6] C.L. Karadimas, T.H. Vu, S.A. Holve, P. Chronopoulou, C. Quinzii, S.D. Johnsen, J. Kurth, E. Eggers, L. Palenzuela, K. Tanji, E. Bonilla, D.C. De Vivo, S. DiMauro, M. Hirano, Navajo neurohepatopathy is caused by a mutation in the MPV17 gene, Am. J. Hum. Genet. 79 (2006) 544–548. https://doi.org/10.1086/506913.

[7] Y.-R. Choi, Y. Bin Hong, S.-C. Jung, J.H. Lee, Y.J. Kim, H.J. Park, J. Lee, H. Koo, J.-S. Lee, D.H. Jwa, N. Jung, S.-Y. Woo, S.-B. Kim, K.W. Chung, B.-O. Choi, A novel homozygous MPV17 mutation in two families with axonal sensorimotor polyneuropathy, BMC Neurol. 15 (2015) 179. https://doi.org/10.1186/s12883-015-0430-1.

[8] M. Baumann, H. Schreiber, B. Schlotter-Weigel, W.N. Löscher, R. Stucka, D. Karall, T.M. Strom, P. Bauer, B. Krabichler, C. Fauth, D. Glaeser, J. Senderek, MPV17mutations in juvenile- and adult-onset axonal sensorimotor polyneuropathy, Clin. Genet. 95 (2019) 182–186. https://doi.org/10.1111/cge.13462.

[9] J.R. Alonzo, C. Venkataraman, M.S. Field, P.J. Stover, The mitochondrial inner membrane protein MPV17 prevents uracil accumulation in mitochondrial DNA, J. Biol. Chem. 293 (2018) 20285–20294. https://doi.org/10.1074/jbc.RA118.004788.

[10] I. Dalla Rosa, Y. Cámara, R. Durigon, C.F. Moss, S. Vidoni, G. Akman, L. Hunt, M.A. Johnson, S. Grocott, L. Wang, D.R. Thorburn, M. Hirano, J. Poulton, R.W. Taylor, G. Elgar, R. Martí, P. Voshol, I.J. Holt, A. Spinazzola, MPV17 Loss Causes Deoxynucleotide Insufficiency and Slow DNA Replication in Mitochondria, PLoS Genet. 12 (2016). https://doi.org/10.1371/journal.pgen.1005779.

[11] A. Spinazzola, C. Viscomi, E. Fernandez-Vizarra, F. Carrara, P. D'Adamo, S. Calvo, R.M. Marsano, C. Donnini, H. Weiher, P. Strisciuglio, R. Parini, E. Sarzi, A. Chan, S. DiMauro, A. Rötig, P. Gasparini, I. Ferrero, V.K. Mootha, V. Tiranti, M. Zeviani, MPV17 encodes an inner mitochondrial membrane protein and is mutated in infantile hepatic mitochondrial DNA depletion, Nat. Genet. 38 (2006) 570–576. https://doi.org/10.1038/ng1765.

[12] C. Dallabona, R.M. Marsano, P. Arzuffi, D. Ghezzi, P. Mancini, M. Zeviani, I. Ferrero, C. Donnini, Sym1, the yeast ortholog of the MPV17 human disease protein, is a stress-induced bioenergetic and morphogenetic mitochondrial modulator., Hum. Mol. Genet. 19 (2010) 1098–107. https://doi.org/10.1093/hmg/ddp581.

[13] A. Trott, K.A. Morano, SYM1 is the stress-induced Saccharomyces cerevisiae ortholog of the mammalian kidney disease gene Mpv17 and is required for ethanol metabolism and tolerance during heat shock, Eukaryot. Cell. 3 (2004) 620–631. https://doi.org/10.1128/EC.3.3.620-631.2004.

[14] R. Reinhold, V. Kruger, M. Meinecke, C. Schulz, B. Schmidt, S.D. Grunau, B. Guiard, N. Wiedemann, M. van der Laan, R. Wagner, P. Rehling, J. Dudek, The Channel-Forming Sym1 Protein Is Transported by the TIM23 Complex in a Presequence-Independent Manner, Mol. Cell. Biol. 32 (2012) 5009–5021. https://doi.org/10.1128/mcb.00843-12.

[15] H. Weiher, T. Noda, D.A. Gray, A.H. Sharpe, R. Jaenisch, Transgenic mouse model of kidney disease: Insertional inactivation of ubiquitously expressed gene leads to nephrotic syndrome, Cell. 62 (1990) 425–434. https://doi.org/10.1016/0092-8674(90)90008-3.

[16] J. Krauss, P. Astrinides, H.G. Frohnhöfer, B. Walderich, C. Nüsslein-Volhard, Transparent, a gene affecting stripe formation in Zebrafish, encodes the mitochondrial protein Mpv17 that is required for iridophore survival, Biol. Open. 2 (2013) 703–710. https://doi.org/10.1242/bio.20135132.

[17] V.D. Antonenkov, A. Isomursu, D. Mennerich, M.H. Vapola, H. Weiher, T. Kietzmann, J.K. Hiltunen, The human mitochondrial DNA depletion syndrome gene MPV17 encodes a non-selective channel that modulates membrane potential, J. Biol. Chem. 290 (2015) 13840–13861. https://doi.org/10.1074/jbc.M114.608083.

[18] E. Bottani, C. Giordano, G. Civiletto, I. Di Meo, A. Auricchio, E. Ciusani, S. Marchet, C. Lamperti, G. D'Amati, C. Viscomi, M. Zeviani, AAV-mediated liver-specific MPV17 expression restores mtdna levels and prevents diet-induced liver failure, Mol. Ther. 22 (2014) 10–17. https://doi.org/10.1038/mt.2013.230.

[19] F. Hagn, M. Etzkorn, T. Raschle, G. Wagner, Optimized phospholipid bilayer nanodiscs facilitate high-resolution structure determination of membrane proteins, J. Am. Chem. Soc. 135 (2013) 1919–1925. https://doi.org/10.1021/ja310901f.

[20] F. Hagn, M.L. Nasr, G. Wagner, Assembly of phospholipid nanodiscs of controlled size for structural studies of membrane proteins by NMR, Nat. Protoc. 13 (2018) 79–98. https://doi.org/10.1038/nprot.2017.094.

[21] K. Klöpfer, F. Hagn, Beyond detergent micelles: The advantages and applications of non-micellar and lipid-based membrane mimetics for solution-state NMR, Prog. Nucl. Magn. Reson. Spectrosc. 114–115 (2019) 271–283. https://doi.org/10.1016/j.pnmrs.2019.08.001.

[22] B. Franke, C. Opitz, S. Isogai, A. Grahl, L. Delgado, A.D. Gossert, S. Grzesiek, Production of isotope-labeled proteins in insect cells for NMR, J. Biomol. NMR. 71 (2018) 173–184. https://doi.org/10.1007/s10858-018-0172-7.

[23] F. Hagn, G. Wagner, Structure refinement and membrane positioning of selectively labeled OmpX in phospholipid nanodiscs, J. Biomol. NMR. 61 (2015) 249–260. https://doi.org/10.1007/s10858-014-9883-6.

[24] P. Zhou, G. Wagner, Overcoming the solubility limit with solubility-enhancement tags:

Successful applications in biomolecular NMR studies, J. Biomol. NMR. 46 (2010) 23–31. https://doi.org/10.1007/s10858-009-9371-6.

[25] I.G. Denisov, Y. V. Grinkova, A.A. Lazarides, S.G. Sligar, Directed Self-Assembly of Monodisperse Phospholipid Bilayer Nanodiscs with Controlled Size, J. Am. Chem. Soc. 126 (2004) 3477–3487. https://doi.org/10.1021/ja0393574.

[26] E. Häusler, K. Fredriksson, I. Goba, C. Peters, K. Raltchev, L. Sperl, A. Steiner, S. Weinkauf, F. Hagn, Quantifying the insertion of membrane proteins into lipid bilayer nanodiscs using a fusion protein strategy, Biochim. Biophys. Acta - Biomembr. 1862 (2020) 183190. https://doi.org/10.1016/j.bbamem.2020.183190.

[27] J. Uusimaa, J. Evans, C. Smith, A. Butterworth, K. Craig, N. Ashley, C. Liao, J. Carver, A. Diot, L. Macleod, I. Hargreaves, A. Al-Hussaini, E. Faqeih, A. Asery, M. Al Balwi, W. Eyaid, A. Al-Sunaid, D. Kelly, I. van Mourik, S. Ball, J. Jarvis, A. Mulay, N. Hadzic, M. Samyn, A. Baker, S. Rahman, H. Stewart, A.A.M. Morris, A. Seller, C. Fratter, R.W. Taylor, J. Poulton, Clinical, biochemical, cellular and molecular characterization of mitochondrial DNA depletion syndrome due to novel mutations in the MPV17 gene, Eur. J. Hum. Genet. 22 (2014) 184–191. https://doi.org/10.1038/ejhg.2013.112.

[28] M. Gilberti, E. Baruffini, C. Donnini, C. Dallabona, Pathological alleles of MPV17 modeled in the yeast Saccharomyces cerevisiae orthologous gene SYM1 reveal their inability to take part in a high molecular weight complex, PLoS One. 13 (2018). https://doi.org/10.1371/journal.pone.0205014.

[29] T. L. Religa, A. M. Ruschak, R. Rosenzweig, L. E. Kay, Site-Directed Methyl Group Labeling as an NMR Probe of Structure and Dynamics in Supramolecular Protein Systems: Applications to the Proteasome and to the ClpP Protease, J. Am. Chem. Soc. 133 (2011) 9063–9068. https://doi.org/10.1021/ja202259a.

[30] I. Goba, D. Goricanec, D. Schum, M. Hillenbrand, A. Plückthun, F. Hagn, Probing the Conformation States of Neurotensin Receptor 1 Variants by NMR Site-Directed Methyl Labeling, ChemBioChem. 22 (2021) 139–146. https://doi.org/https://doi.org/10.1002/cbic.202000541.

[31] A. Steiner, K. Schlepckow, B. Brunner, H. Steiner, C. Haass, F. Hagn, γ-Secretase cleavage of the Alzheimer risk factor TREM2 is determined by its intrinsic structural dynamics, EMBO J. 39 (2020) e104247. https://doi.org/https://doi.org/10.15252/embj.2019104247.

[32] O. Teijido, R. Ujwal, C.O. Hillerdal, L. Kullman, T.K. Rostovtseva, J. Abramson, Affixing N-terminal α-helix to the wall of the voltage-dependent anion channel does not prevent its voltage gating, J. Biol. Chem. 287 (2012) 11437–11445. https://doi.org/10.1074/jbc.M111.314229.

[33] P.L. Privalov, Stability of proteins: Small Globular Proteins, Adv. Protein Chem. 33 (1979) 167–241. https://doi.org/10.1016/S0065-3233(08)60460-X.

[34] M. Salzmann, K. Pervushin, G. Wider, H. Senn, K. Wüthrich, Trosy in triple-resonance experiments: New perspectives for sequential NMR assignment of large proteins, Proc. Natl. Acad. Sci. U. S. A. 95 (1998) 13585–13590. https://doi.org/10.1073/pnas.95.23.13585.

[35] S.G. Hyberts, K. Takeuchi, G. Wagner, Poisson-gap sampling and forward maximum entropy reconstruction for enhancing the resolution and sensitivity of protein NMR data, J. Am. Chem. Soc. 132 (2010) 2145–2147. https://doi.org/10.1021/ja908004w.

[36] S.G. Hyberts, A.G. Milbradt, A.B. Wagner, H. Arthanari, G. Wagner, Application of iterative soft thresholding for fast reconstruction of NMR data non-uniformly sampled with multidimensional Poisson Gap scheduling, J. Biomol. NMR. 52 (2012) 315–327. https://doi.org/10.1007/s10858-012-9611-z.

[37] F. Delaglio, S. Grzesiek, G.W. Vuister, G. Zhu, J. Pfeifer, A. Bax, NMRPipe: a multidimensional spectral processing system based on UNIX pipes, J. Biomol. NMR. 6 (1995) 277–293. http://www.ncbi.nlm.nih.gov/pubmed/8520220.

[38] W. Lee, M. Tonelli, J.L. Markley, NMRFAM-SPARKY: enhanced software for biomolecular NMR spectroscopy, Bioinformatics. 31 (2015) 1325–1327. https://doi.org/10.1093/bioinformatics/btu830.

[39] Y. Shen, F. Delaglio, G. Cornilescu, A. Bax, TALOS+: a hybrid method for predicting protein backbone torsion angles from NMR chemical shifts, J. Biomol. NMR. 44 (2009) 213–223. https://doi.org/10.1007/s10858-009-9333-z.

[40] F. Hagn, C. Klein, O. Demmer, N. Marchenko, A. Vaseva, U.M. Moll, H. Kessler, BclxL

changes conformation upon binding to wild-type but not mutant p53 DNA binding domain, J. Biol. Chem. 285 (2010). https://doi.org/10.1074/jbc.M109.065391.

Figure captions

Fig. 1. Optimization of the production and refolding of MPV17 produced in *E. coli*. (a) MPV17 is an inner mitochondrial membrane protein potentially involved in nucleotide precursor transport and ROS signaling. (b) MPV17 could only be produced in *E. coli* cells as a fusion protein with GB1. MPV17 inclusion bodies were purified in chemical denaturants and refolded into detergent micelles. (c) Representative SEC S200 profile of refolded MPV17 after thrombin cleavage of the GB1 fusion protein. Due to the attached His_6-tag and a linker, GB1 runs at 17 kDa. (d) SDS-PAGE of the SEC fractions labeled in (c). Minor bands visible in the gel originate from uncleaved GB1-MPV17 (30 kDa) or dimeric MPV17 (40 kDa). IM: inner membrane; OM: outer membrane; H: His-tag; T: thrombin site; L: GGSS linker; GuHCl: guanidine hydrochloride; M: molecular weight marker.

Fig. 2. Detergent screening and NMR evaluation with MPV17. (a) Far-UV CD spectra of MPV17 in the indicated detergents at 20 °C. (b) CD-detected thermal melting curves of MPV17 in different detergents. (c) Thermal melting curves of MPV17 refolded into DPC micelles and reconstituted in DMPC:DMPG (4:1) liposomes. (d) 2D-[^{15}N, ^{1}H]-TROSY spectra of *U*-[^{2}H,^{15}N]-labeled MPV17 in the indicated detergents at 37 °C. Best NMR spectral quality was obtained in DPC micelles.

Fig. 3. NMR backbone resonance assignment and dynamics of ^{2}H,^{13}C,^{15}N-labeled MPV17 in DPC micelles. (a) 2D-[^{15}N,^{1}H]-TROSY spectrum of MPV17 with assigned backbone amide resonances labeled. 89% of all non-proline residues in the protein could be assigned. (b) Representative strips of a 3D-TROSY-HNCA experiment that was used to obtain sequence specific backbone resonance assignments. (c) Secondary chemical shift data analysis of MPV17 in DPC micelles indicates six α-helical segments. (d) {^{1}H}-^{15}N heteronuclear NOE data (low value for dynamic and high values for rigid regions in the protein in the ns to ps time scale) data of MPV17 correlates well with the presence of secondary structure elements. For comparison, the predicted order parameter pattern calculated from chemical shift information is shown as a black line. (e) Degree of sequence conservation among mammalian MPV17 homologues using human, macaque, bovine, bison, seal, hedgehog, mouse and rat amino acid sequences with a sequence conservation of > 90%. Sequence variability is mainly observed in regions outside secondary structure elements.

Fig. 4. Membrane location of MPV17 helices probed with NMR paramagnetic relaxation enhancement (PRE) experiments. (a) 2D-[^{15}N,^{1}H]-TROSY spectra of MPV17 in DPC micelles and after addition of 8 mM Gd^{3+}-chelated DOTA (b) same as in (a) but with 1 mM 16-doxyl stearic acid (16-DSA). (c) Intensity plot of the NMR signals in (a) before and after the addition of the water-soluble DOTA chelator loaded with paramagnetic Gd^{3+} which affects the intensity of solvent-exposed residues in MPV17 via PRE. (d) Intensity ratio with 1 and 2 mM 16-DSA, a spin-labeled fatty acid

that affects residues of MPV17 that are located inside the detergent micelle. Negative bars indicate missing resonance assignments.

Fig. 5. Lipid nanodisc incorporation of MPV17. (a) Overview of the nanodisc assembly procedure. The GB1-MPV17 fusion construct is assembled into nanodiscs out of DPC micelles. Finally, the GB1 is cleaved off resulting in a 1:1 stoichiometric ratio between GB1 and incorporated MPV17. (b) SEC profiles of different MPV17 constructs incorporated into nanodiscs after GB1 cleavage. The nanodiscs and GB1 are well separated, so that the amount of GB1 can be directly used to calculate the amount of MPV17 per nanodisc. Top: MPV17ΔCys in ΔH5-nanodiscs. Bottom: met-MPV17wt in ΔH5-nanodiscs. (c) Far-UV CD melting curves of the different MPV17 constructs in ΔH5-nanodiscs. (d) Overview of the different MPV17 nanodisc assemblies. The assembly ratios, lipids and MSP constructs were varied resulting in similar amounts of MPV17 per disc for both MPV17 samples. (e) 2D-[^{15}N,^{1}H]-TROSY spectrum of MPV17ΔCys in ΔH5-nanodiscs formed with DMPC/DMPG-lipids (blue) overlayed with the MPV17ΔCys spectrum in DPC micelles.

Fig. 6. NMR and protein folding analysis of cysteine-free and cysteine-modified MPV17. (a) Overlay of 2D-[^{15}N,^{1}H]-TROSY spectra of MPV17wt (black) and cysteine-methylated MPV17wt (green) in DPC micelles. (b) same as in (a) but with cysteine-free MPV17 (red). (c), (d) NMR chemical shift perturbation plots of met-MPV17wt (c) and MPV17-cysfree (d) using MPV17wt as a reference. (e,f) Thermal unfolding transitions of MPV17wt (e) and cysteine-free (f) in DPC micelles monitored by CD spectroscopy at 222 nm.

Fig. 7. MPV17 form covalent oligomers in a cysteine-dependent manner. (a) Cysteine-mediated oxidative crosslinking of MPV17 with (o-phenanthroline)$_2$-Cu^{2+} in DPC micelles and liposomes. Higher oligomers can only be observed in liposomes. (b) Amino selective crosslinking of MPV17 in DPC micelles and liposomes with BS^3 with or without the reducing agent DTT. (c) 2D-[^{15}N,^{1}H]-TROSY spectra of MPV17wt in presence and absence of 5 mM DTT. MPV17 readily forms larger species if DTT is omitted giving rise to signal disappearance and line broadening in the NMR spectra. Signals that are disappearing in the oxidized sample are marked in the reduced sample spectrum. (d) NMR signal intensity plot of the spectra shown in (c). A marked reduction in the signal intensity is observed in regions where cysteine residues are present, further supporting a cysteine-dependent oligomerization mechanism. Negative bars indicate missing signals or resonance assignments. (e) Nanodisc assembly with MPV17wt and disease-linked variants. MPV17wt forms oligomers and does not fit into nanodiscs, whereas the MPV17 variants can be inserted into nanodiscs, suggesting a less pronounced tendency for oligomerization. The GB1-cleavage assay to determine the number of MPV17 monomers in the nanodiscs gives values very close to one, which is lower than for cysteine-free MPV17 (see Fig. 5).

Fig. 8. Model of MPV17 functionality of redox-dependent oligomeric pore formation. Reactive oxygen species (ROS) are a byproduct of oxidative phosphorylation in the respiratory chain in mitochondria. Enhanced levels of ROS lead to DNA damage and eventually to a lack of protein expression of respiratory chain complexes that are encoded by mitochondrial DNA (mito-DNA). MPV17, also located in the inner mitochondrial membrane, is able to sense oxidative stress via its cysteine residues, leading to the formation of a stable oligomeric pore that can serve as an entry channel for nucleotide precursors that are required for mito-DNA synthesis and repair. This model can explain the severe effects of MPV17 leading to mitochondrial DNA depletion, mitochondrial misfunction and associated phenotypes such as liver failure in early childhood. OMM: outer mitochondrial membrane, IMM: inner mitochondrial membrane, IMS: inter membrane space. Ox. Phos.: components of the respiratory chain, esp. complex IV, where electron transfer to O_2 takes place.

Figures

Figure 1

-

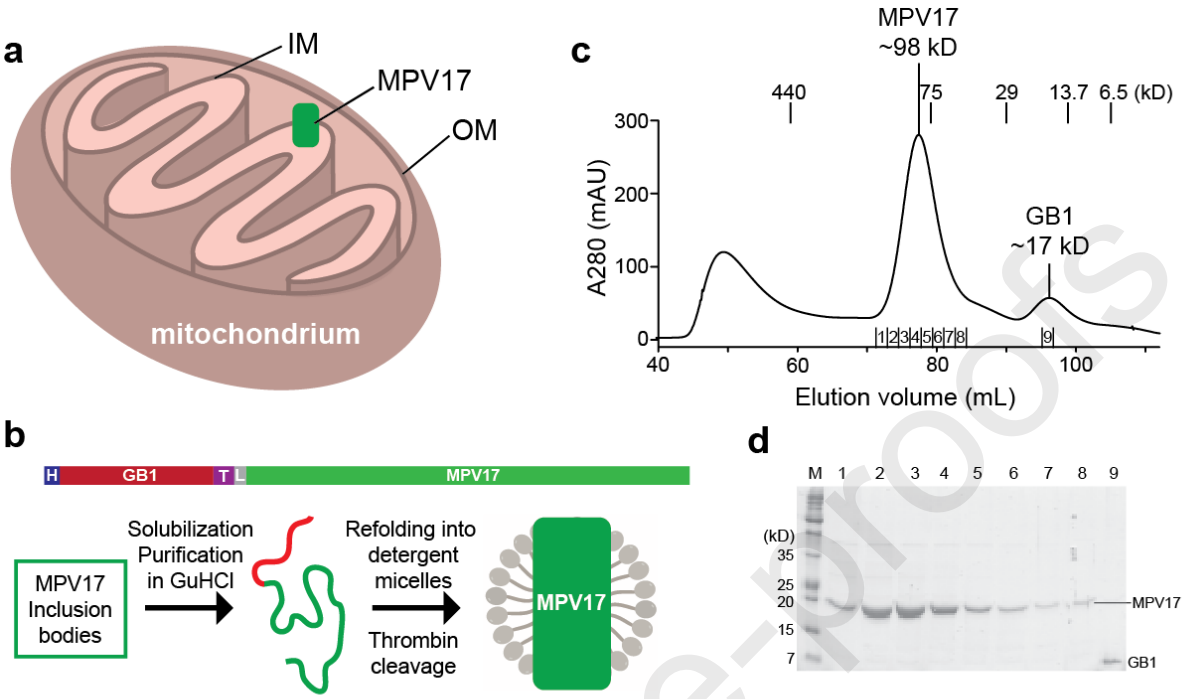

Figure 2

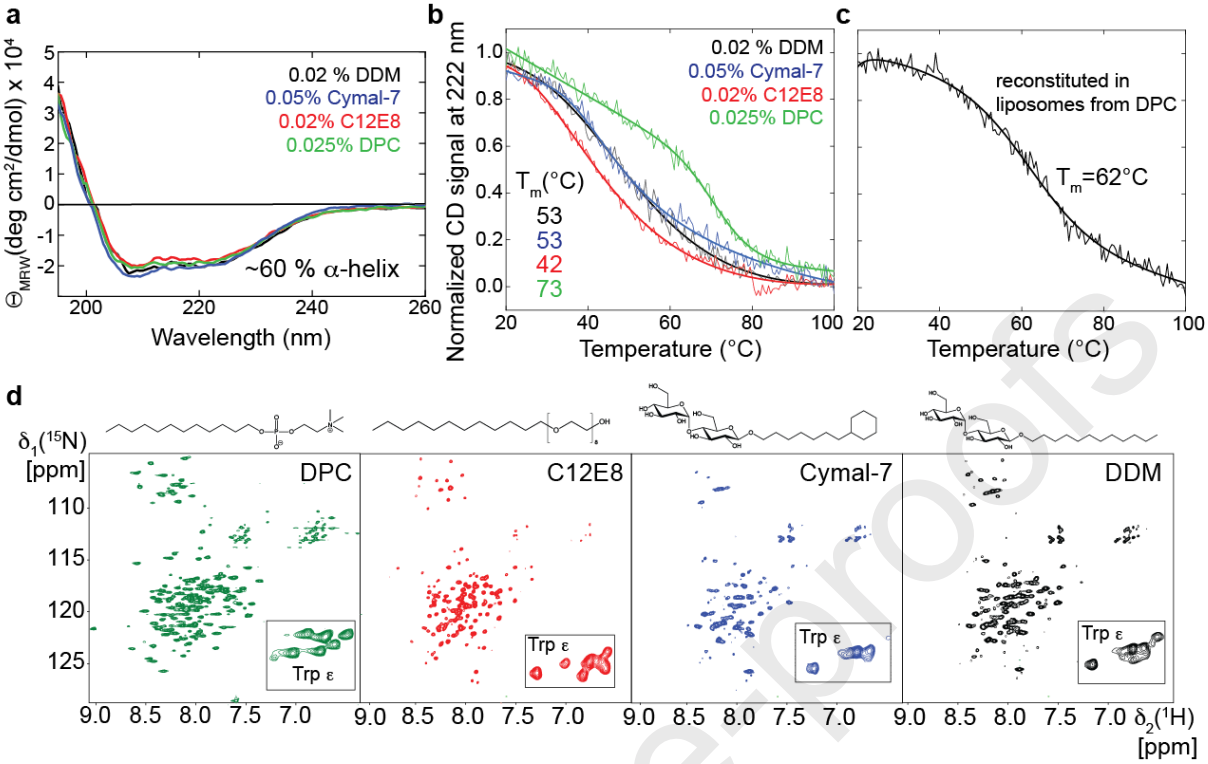

Figure 3

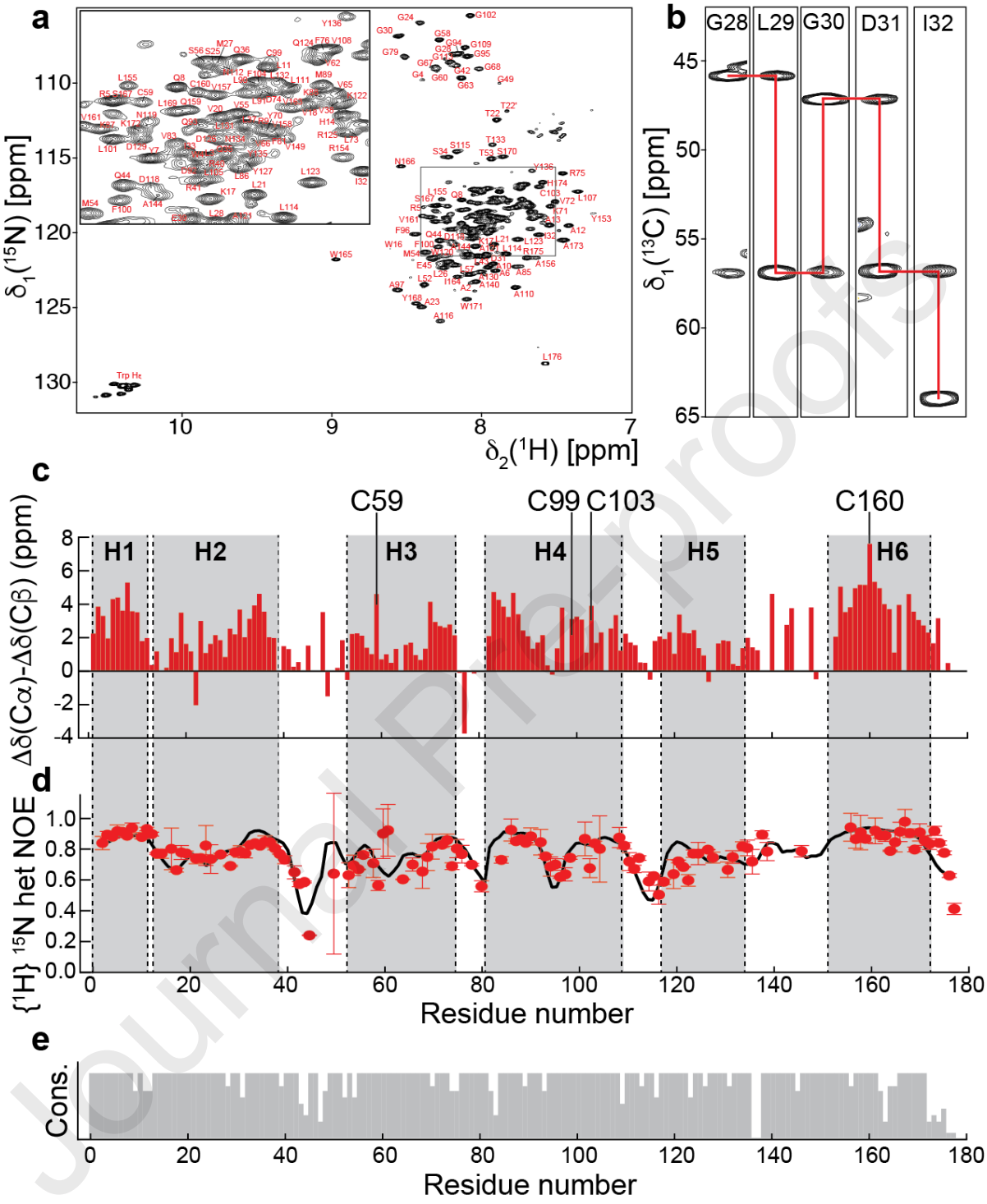

Figure 4

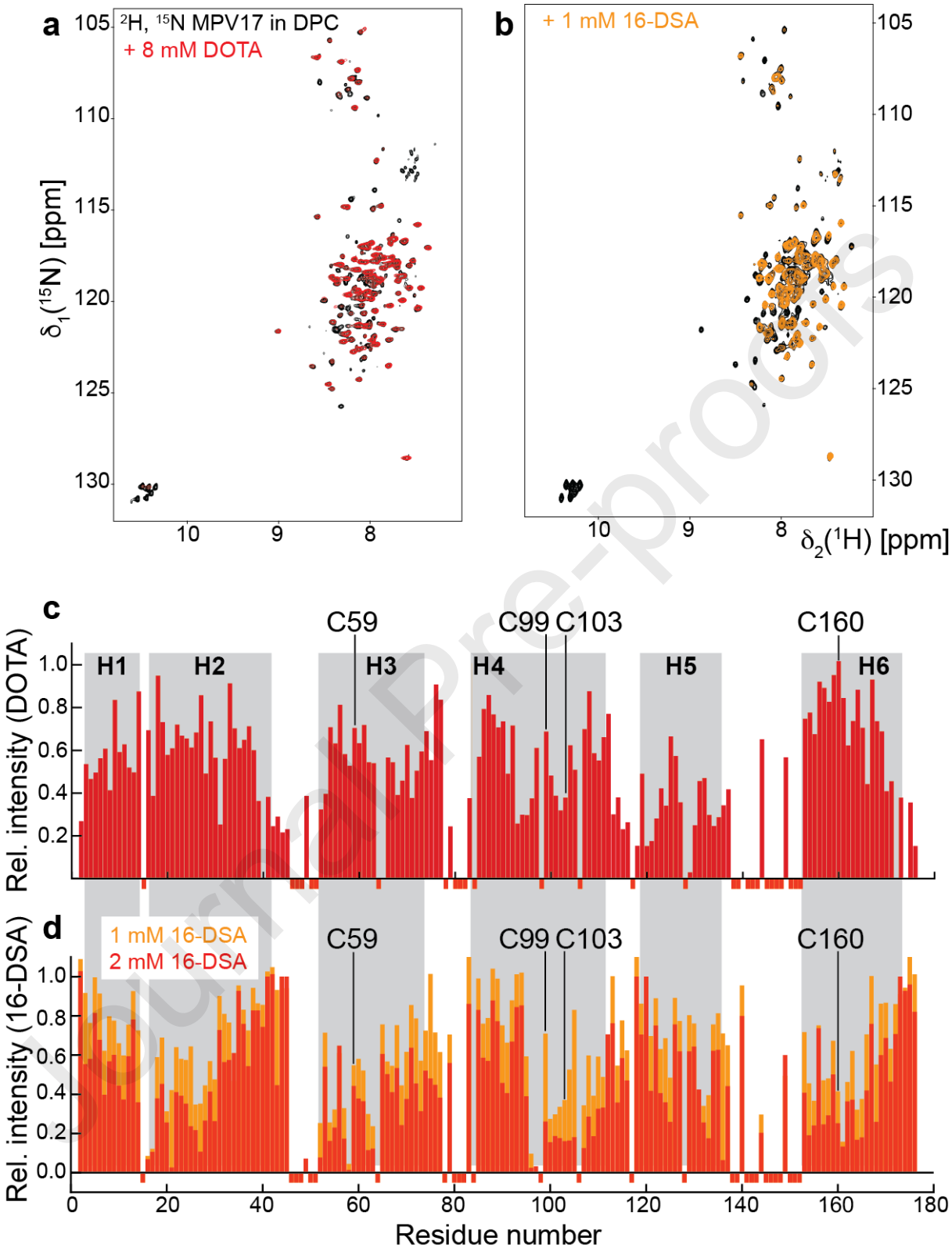

Figure 5

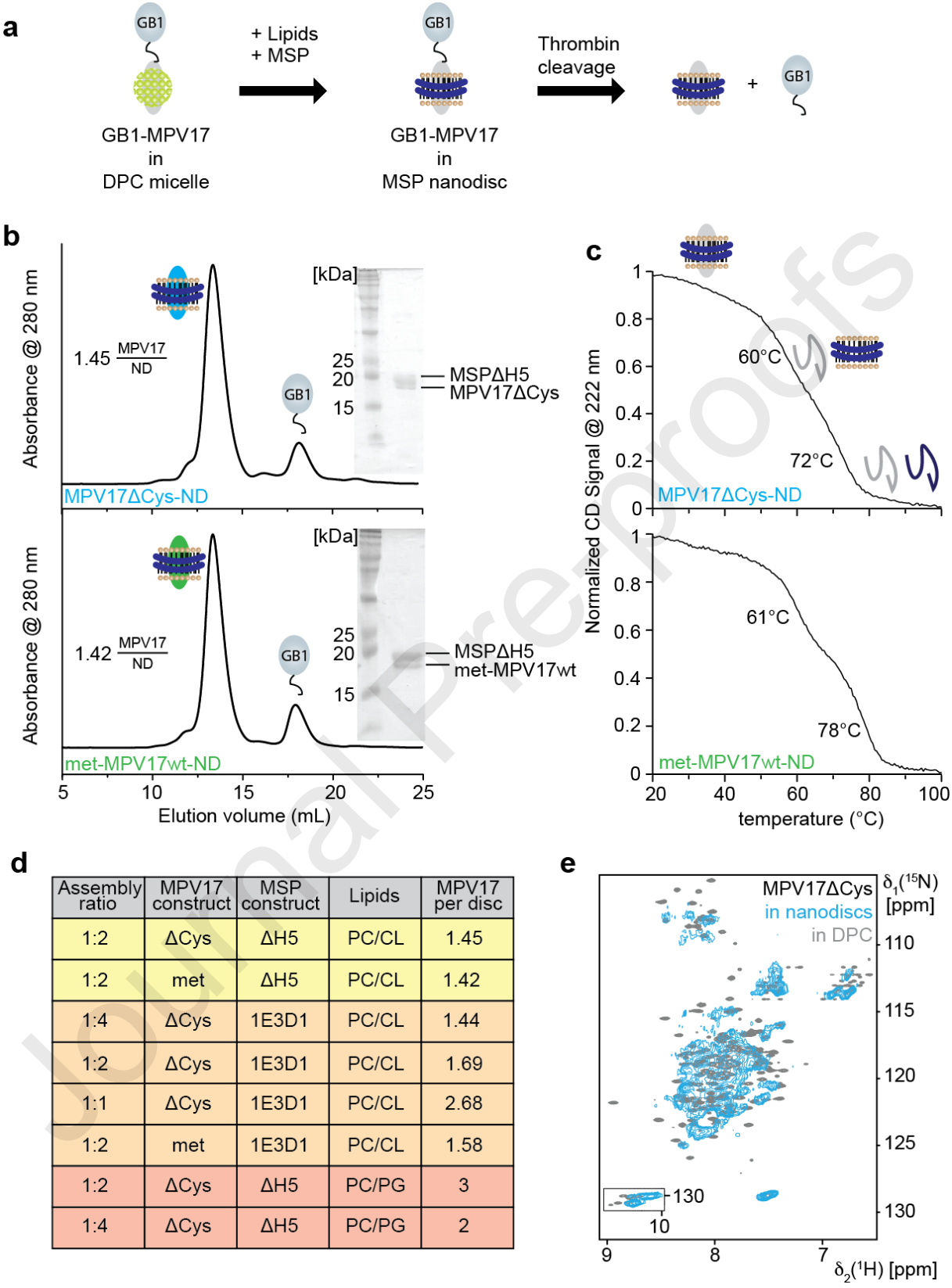

Assembly ratio	MPV17 construct	MSP construct	Lipids	MPV17 per disc
1:2	ΔCys	ΔH5	PC/CL	1.45
1:2	met	ΔH5	PC/CL	1.42
1:4	ΔCys	1E3D1	PC/CL	1.44
1:2	ΔCys	1E3D1	PC/CL	1.69
1:1	ΔCys	1E3D1	PC/CL	2.68
1:2	met	1E3D1	PC/CL	1.58
1:2	ΔCys	ΔH5	PC/PG	3
1:4	ΔCys	ΔH5	PC/PG	2

Figure 6

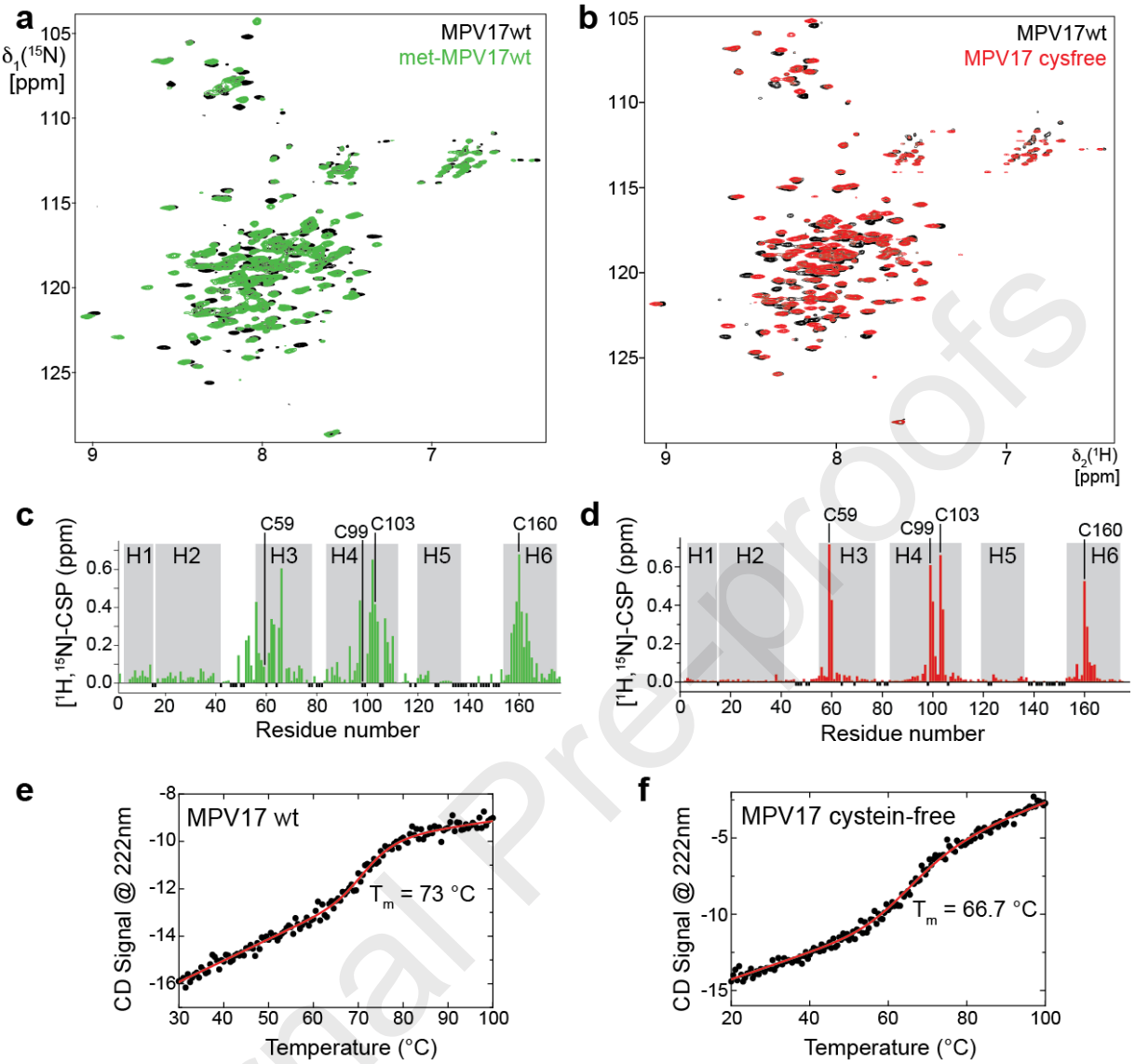

Figure 7

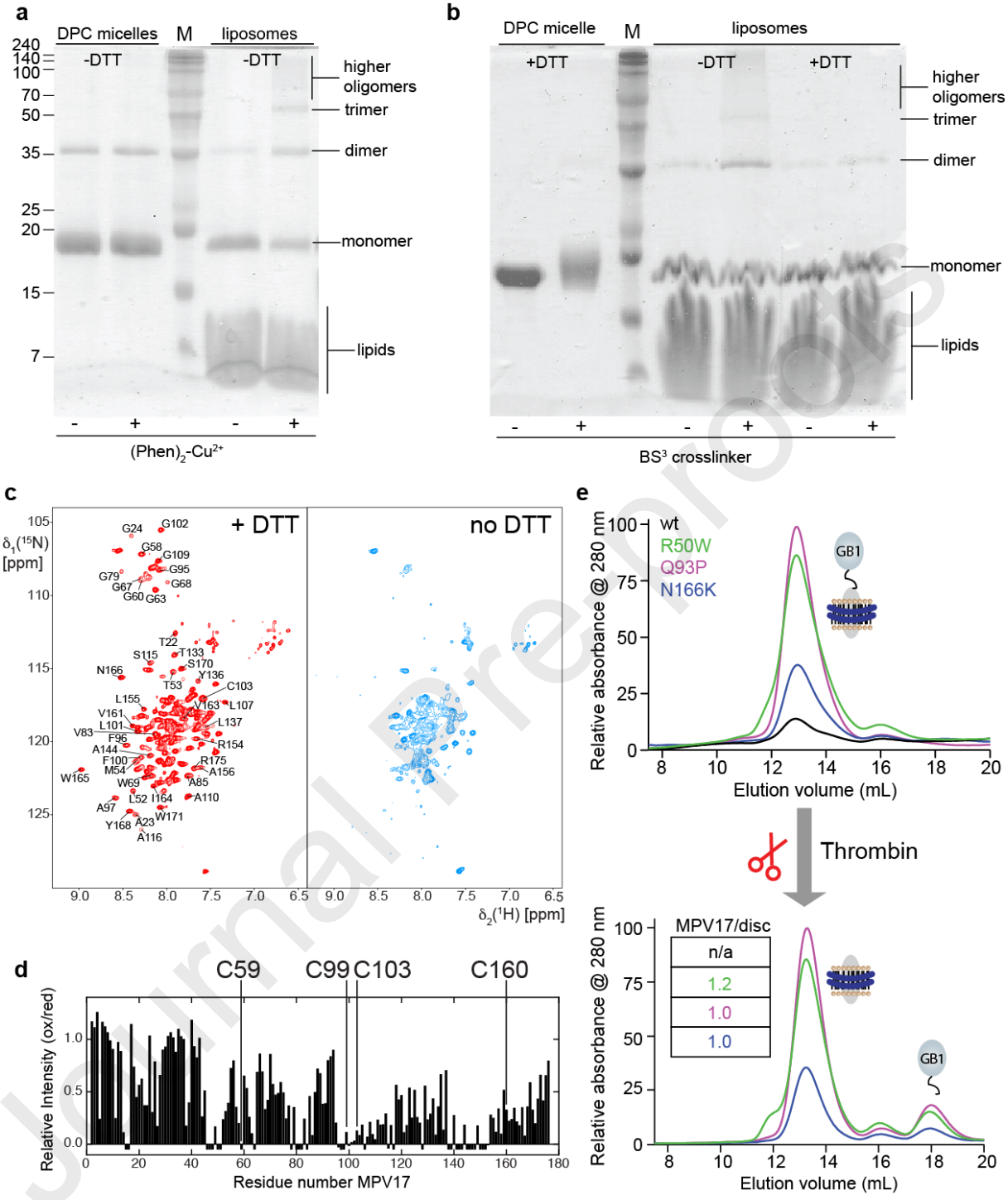

Figure 8

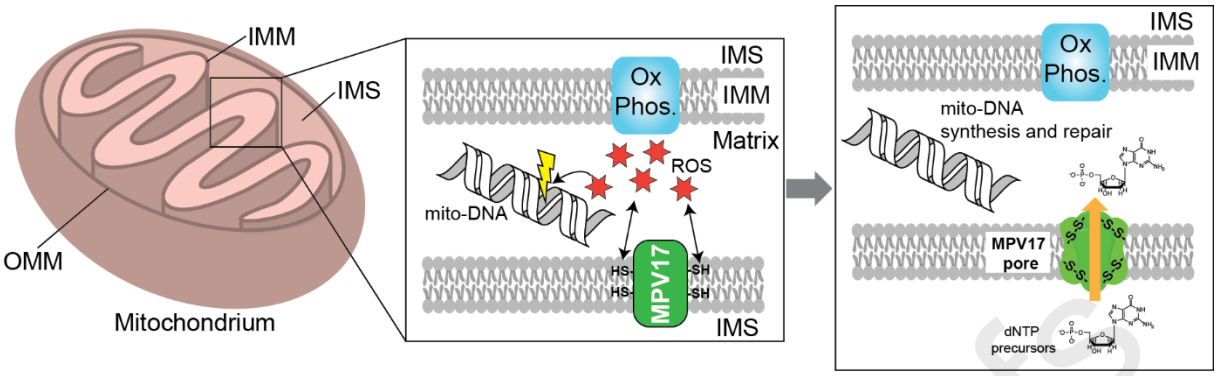

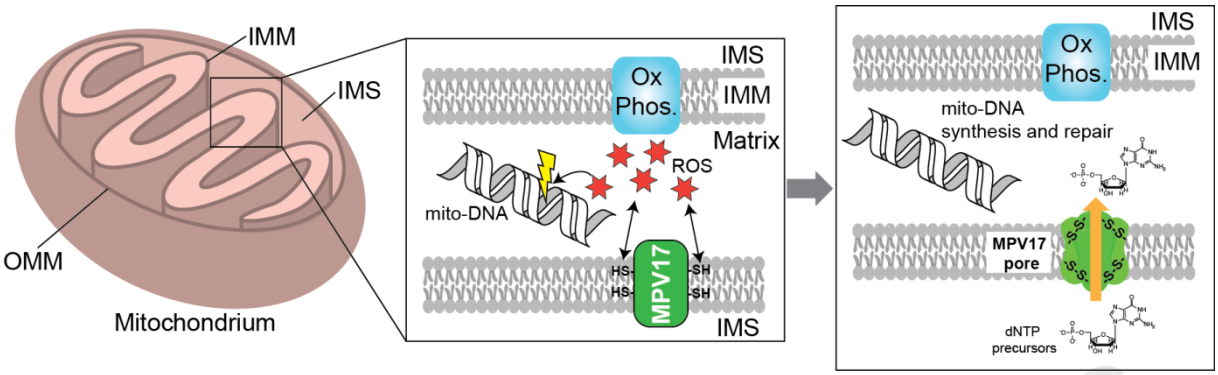

Research Highlights

- Structural and functional features of the inner mitochondrial disease-linked protein MPV17 are only poorly understood.

- Establishment of MPV17 production in *E. coli* and screening for suitable detergents for structural and biophysical studies.

- NMR resonance assignment, secondary structure content, dynamics and membrane location of MPV17 in DPC micelles.

- Lipid nanodisc assay to determine the tendency of MPV17 to form larger oligomers, which can be inhibited by the removal of cysteine residues or by the introduction of disease-linked mutations.

- These data provide first structural insights into MPV17 and suggest that this protein is a redox sensor that forms oligomeric pores upon expose to oxidative stress.

Laura E. Sperl: Conceptualization, Methodology, Validation, Investigation, Resources, Writing- Review and editing, Project administration.

Franz Hagn: Conceptualization, Investigation, Writing- Original draft preparation, Visualization, Supervision, Project administration, Funding acquisition.